博士論文 （要約）

Doctoral thesis

Experimental Investigation of Cellulose-based Nanostructures with Promoted Thermal Conductivity

(熱伝導率促進型のセルロースナノ構造体の実験的研究)

王冠瞳

WANG GUANTONG

指導教員：塩見淳一郎 教授

令和 3 年 12 月

Abstract

To curb the emission of carbon dioxide and control the global warming, it is pertinent to develop innovative materials and technologies using renewable resources. Cellulose is regarded as a green and renewable resource that has attracted attention in recent years due to its excellent mechanical properties. Cellulose can be obtained from many kinds of plant resources such as wood and stems. Although the mechanical properties of such cellulose materials are well investigated, research on understanding the thermal properties of such materials is at an early stage. The thermal conductivity of cellulose materials has not been fully investigated yet since it strongly depends on the structure, purity content, and morphology, etc. To explore the use of cellulose-based materials in industrial applications, it is important to investigate their thermal properties in detail.

In the first work of this thesis, we obtained cellulose filaments with the diameter ranging from 6-18 um utilizing two kinds of fabrication conditions (with hydrochloric acid and ferric chloride). We developed a flow-focusing channel system [1] to enhance the thermal conductivity of cellulose filaments by controlling the alignment, crystalline nature and orientation. The cellulose nano-fibrils dispersed in deionized water are processed by the flow focusing channel, where cellulose nano-fibrils get hydrodynamically aligned along the flow direction. In addition, salt or acid is added into the channel, which makes the cellulose filaments become gelled by forming hydrogen bonding or ionic bonding.

The thermal conductivity of individual filaments is measured using a custom-built T-type measurement technique. Our results show that the highest thermal conductivity of cellulose filament reaches 14.5 ± 0.49 W/m-K. Smaller diameter filaments show higher thermal conductivity due to the formation of high crystallinity regions during the gelation process, which is confirmed by Raman spectroscopy. In addition, we found that residual stress produced during the gelation process lead to a

decrease in crystallinity, which in turn decreases thermal conductivity. Filaments gelled with hydrochloric acid show higher thermal conductivity compared to the case of ferric chloride, mainly attributed to the formation of high crystalline regions due to increased covalent bonding which is confirmed by the Raman spectroscopy results.

In the second part of the thesis, we investigated thermal conductivity of cellulose based composite for fire retardant applications and reports the results of anisotropic ratio of thermal conductivity. Wood, which is composed of cellulose, is widely used in building systems mainly due to its lightweight and strong mechanical properties. However, cellulose is flammable, which brings hidden danger to the safety of buildings. Most of the flame-retardant materials contain bromine and chlorine that are reported to form toxins. On the other hand, a new green functional flame retardant material, montmorillonite-clay is widely used due to its excellent mechanical properties, gas barrier properties, biodegradability, and flame retardant properties. However, the thermal conductivity of pure montmorillonite clay is low, which is problematic for its application. One possible solution is to improve the thermal conductivity of pure montmorillonite clay by adding high thermal conductivity materials. Nano-cellulose is generally introduced for its high strength and high crystalline nature to improve composites' mechanical and thermal properties.

With the inspiration based on the high thermal conductivity cellulose filaments obtained from the experiments, we aimed to expand its application to a larger scale. For this, we performed anisotropic thermal conductivity measurements of films of a layer-by-layer hierarchical structure of Montmorillonite-clay/cellulose nanocomposite with thickness around 90 μm fabricated by vacuum-filtration and drying. Montmorillonite platelets act as ‘brick’ with a thickness of around 1.1 nm, and nano-cellulose acts as ‘mortar’ with 3 nm in diameter and several micrometers in length[2]. The aim is to realize a composite with a relatively high anisotropy ratio of thermal conductivity, to decrease the localization of high temperature. We measured the anisotropy ratio of thermal conductivity as a function of montmorillonite-clay/cellulose content using the

laser flash technique. Our result shows that the cross-plane thermal conductivity depends on the clay content non-monotonically; as the clay content increases from 0% (pure cellulose), the thermal conductivity decreases until the content reaches 80% and then increases until 100%. The in-plane thermal conductivity also shows a non-monotonic dependence on the content; increasing to 50 % and then decreasing. This gives rise to the largest anisotropy for clay content of 50 %, where in-plane thermal conductivity is 30 times larger than the cross-plane thermal conductivity. Furthermore, Raman spectroscopy was performed to investigate the orientation of cellulose nano-fibrils in the composite, and the analysis reveals that the degree of alignment strongly depends on the clay content with the maximum achieved at 50 % content and the large anisotropy is originated from the alignment of the cellulose nano-fibrils.

TABLE OF CONTENTS

Chapter 1 Introduction

With the ever-increasing emission of carbon dioxide, the total emission of carbon dioxide has reached over 30,000 million tons until 2013 globally [2] resulting in global warming and climate change. The general ways to decrease carbon emission are finding other alternative materials to replace fossil fuels products, energy-saving or planting trees, etc.

Cellulose is a kind of renewable resource which is environmentally friendly, lightweight, economical to produce, and possesses excellent mechanical properties [3]. Cellulose, $(C_6H_{10}O_5)_n$ is an organic polysaccharide compound, with thousands of glucose units. It is an important part of the primary cells of plants, algae, and oomycetes. It has been widely used in paper, glass fibers, and so on. Currently, the use of cellulose in energy-saving products, such as rayon and cellulosic ethanol have drawn attention in industries.

With good performance and its abundance of resources of cellulose materials, a lot of new cellulose-based products have been utilized during the past decade. To expand its utilization in the market, a key physical property namely the thermal property has to be clearly understood. For instance, in building systems, lot of wood-based materials are used, due to their high strength, lightweight properties, however, the thermal property of wood is not good enough so that it becomes uncomfortable for living conditions in building systems. Therefore, it is interesting and challenging to investigate the thermal properties of cellulose-based materials for applications in thermal management of electronics, fire retardant materials and so on.

1.1 Cellulose materials and their properties.

Cellulose can be obtained from many kinds of plant resources such as wood and stems, tunicates and even in bacteria. However, plants, especially wood, is the

main resources for cellulose in industry, as the content for cellulose in wood is around 50% [4]. With the high content of cellulose and abundance of resources in nature, wood becomes a promising resource for the cellulose industry. Wood is composed of about 45% cellulose, 30% hemicellulose, and 25% lignin regions. In the cross-section of a tree, the growth of the ring covers the area with the circular point in the middle of the geometric center. Along with the millimeter size of the growth ring, cellulose cell walls grow along the longitudinal direction of the fiber. Inside the cellulose cell wall, the fibril structures appear with the unit size of several hundred nanometers. The nanometer size fibrils are composed of elementary fibrils, which are the combination of crystalline regions (with 5-20 nm in width and ~500 nm in length) and amorphous regions[5,6].

Cellulose is the main part inside the cell wall and exhibits many advantages such as being environmentally friendly and excellent mechanical properties [4]. Excellent mechanical performance, such as low density (≈ 1.5 g/cm^3), high strength (1.6-3 GPa), and high crystalline stiffness (≈ 130 GPa) have drawn researchers significant attention [5]. Cellulose was first found by a French scientist, Anselme Payen, who extracted it from plants and figured out its structure unit. Since then, companies all over the world put great effort into their production, and the first successful product was made by Hyatt Manufacturing Company in 1870. Since then, a lot of products have been produced and commercialized, as ink dispersant components in ballpoint pens with relatively good quality of writing performance[6], and a kind of disposable diapers with deodorizing functions for health care assistants[6].

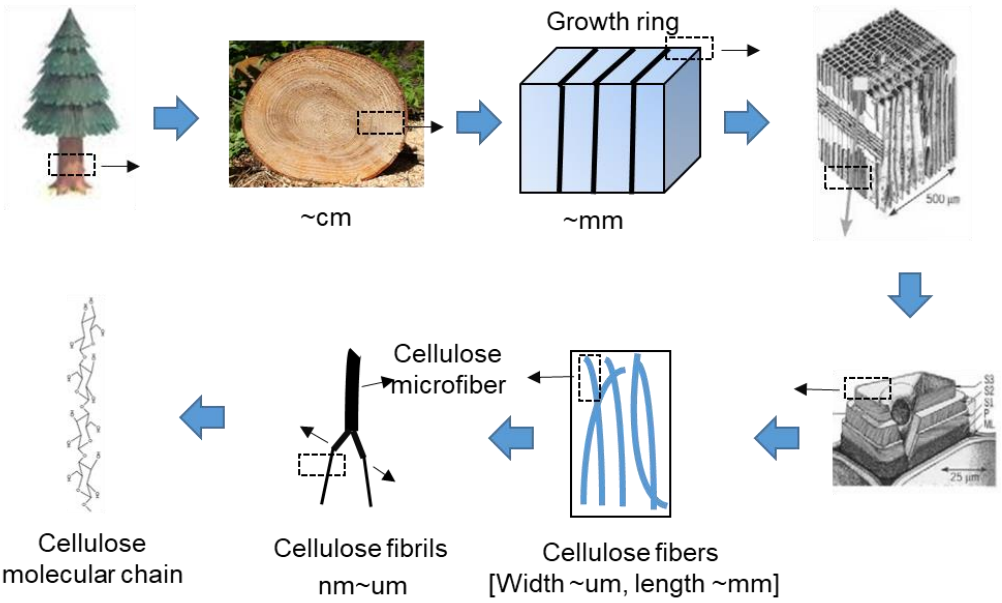

Fig. 1 Basics of cellulose with hierarchical structure obtained from wood. The size of each element range from meter level to nanometer level [5,6].

With better performance and various commercialized products of cellulose mentioned above, it is interesting and challenging to find more advanced properties, which could help enlarge the application of cellulose-based materials, for instance, thermal properties, that could contribute to the application in building systems.

To understand the thermal properties of nano-cellulose, we start to understand the structure of the cellulose molecular chain. Along the cellulose molecular chain, the rocking hydroxyl or carboxyl (in the case of TEMPO CNF explained below) could form interactions (in cellulose dispersion, the charged hydroxyl or carboxyl groups form electrostatic repulsion between fibrils) between fibril and fibril and build connections (such as hydrogen bonds) that contribute to the thermal, mechanical, electric, magnetic properties when the molecular chain is along with the direction of the fibrils. For the controllability of the orientation of cellulose filaments, it is important to separate individual fibrils first so that they can be used as building blocks.

Since the cellulose fibrils obtained directly from wood pulp contain a lot of interactions between fibrils, to separate cellulose fibrils, usually researchers use acid hydrolysis or enzyme hydrolysis methods[7]. However, the methods could not work completely to obtain individual cellulose fibrils until Isogai-Saito group in the

University of Tokyo successfully fabricated TEMPO-CNF fibrils with 4 nm in diameter and several hundred nm in length in 2006 [8].

Generally, TEMPO cellulose is obtained from oxidation of cellulose analogs with potassium bromide or sodium hypochlorite under PH at 10-11 alkaline solutions[9,10]. First of all, non-TEMPO cellulose dispersion is decentralized in distilled water, and cellulose which is structured with alcohol hydroxyl groups, are oxidized into aldehyde structures, following into ketone structures, and finally into carboxyl structures with the catalytic reaction with the help of sodium bromide. The oxidizing reaction happens in the reaction by sodium hypochlorite, with the catalytic reaction by sodium bromide under alkaline conditions (PH 10-11)[8]. The basic reaction flow diagram is summarized below. The final TEMPO cellulose is rod-like structure with several micrometers in length and from 3-4 nanometers in diameter. However, the thermal conductivity of individual cellulose fibrils has not been fully understood.

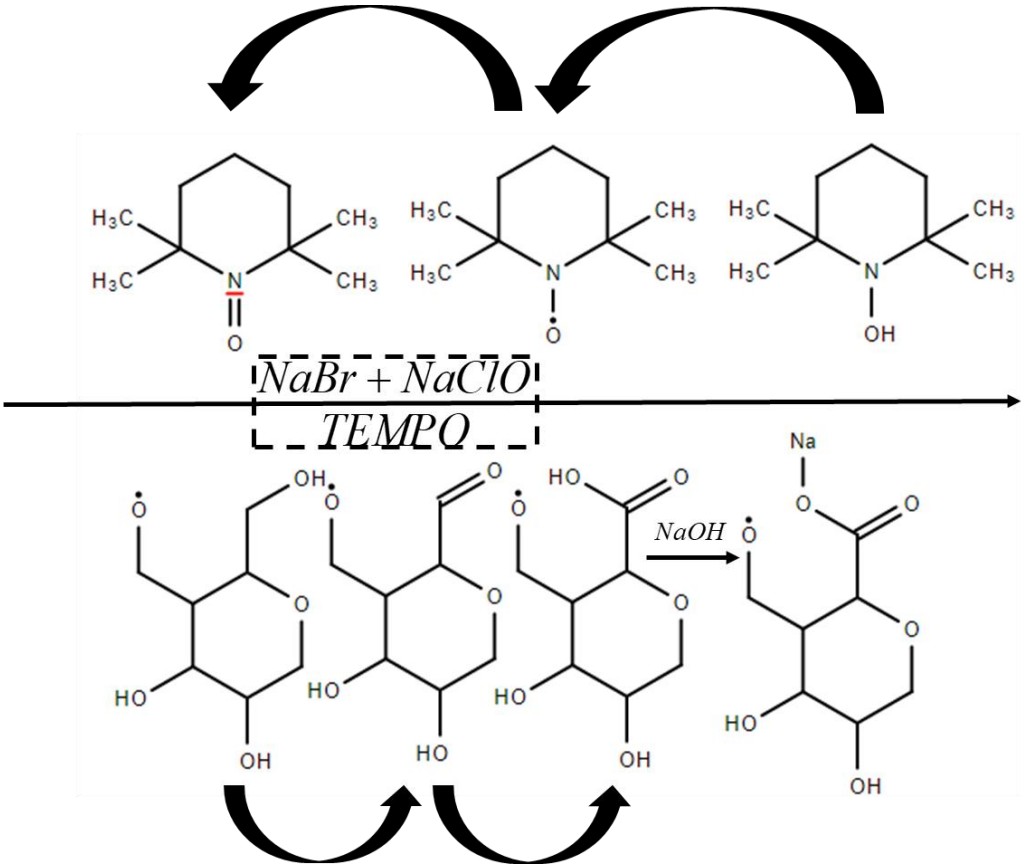

Fig. 2 Basic reaction flow diagram of TEMPO cellulose at PH 10-11 conditions[8].

1.2 Thermal management materials.

The increasing use of micro-electronics in industries and home appliances has made our daily lives comfortable. However, overheating problems becomes one of the barriers for electronic devices, which have limited the further use of products[9]. To ensure the good working performance of products, overheating problems need to be solved. A lot of works have been done in designing good heat sinks to dissipate heat effectively in the field of thermal management. The typical materials used in thermal management in electric devices are active and passive cooling materials. For active cooling, it is used to dissipate heat through external devices which are connected with heat sources, such as heat sink[10]. However, active cooling needs large systems which are more energy-consuming. For the passive cooling systems, the heat dissipation relies on the properties of the material and doesn't require a complicated system, and additional energy consumption. The efficiency strongly depends on the thermal properties of materials. Cellulose shows good mechanical properties, and its composite materials have been used as structural supports materials for electronic devices. However, the thermal properties of cellulose have not been investigated in detail yet which is the scope of this work.

1.3 Approaches to improve the thermal conductivity of cellulose materials.

To know the thermal conductivity of cellulose fibrils, filaments, or composites, first, it is vital to know the thermal performance of individual fibrils. The study conducted by [11] report that the thermal conductivity of individual fibrils (with diameter is several nm, and length is several um) was found at 2.2 ± 1.2 W/m-K, which was measured by the thermal bridge method. In terms of polymer chain, Shrestha et al. [17], measured the thermal conductivity of polyethylene fibrils with diameter from 10-100 nm. The result shows that the thermal conductivity increases from the temperature

range below 100 K and reaches a high thermal conductivity at 90 W/m-K and then decreases monotonously with increasing temperature. They obtained high crystalline nature with micrometer level polyethylene fibrils via stretching and heating (micro heater) for the whole fibers. By applying these methods, the amorphous regions in the fibrils could become aligned and realigned in the defect areas, and indeed, the crystalline regions become larger.

Another interesting work done by Xu et. al [12] shows that the thermal conductivity of polyethylene film can reach as high as 62 W/m-K which is over hundreds of times higher than traditional polymer thermal conductivity. In their work, they started with powder of polyethylene which is semi-crystalline. Next, they dissolved the powder and dispersed it in solution, then applied high temperature to melt the powder and extrude the films with the help of liquid nitrogen. Via applying drawing along with the orientation of fibrils direction, the amorphous regions could be further improved into transition regions, and then into crystalline regions. Interestingly, with the drawing ratio increase, the thermal conductivity along with in-plane direction increased monotonously, and the highest thermal conductivity was found at 60 W/m-K when the drawing ratio reached 110 times. The thermal conductivity of amorphous regions also shows a monotonous increase of thermal conductivity with an increasing drawing ratio. The highest thermal conductivity was found at 15 W/m-K when the drawing ratio reaches 110 times. Furthermore, the findings (high crystalline orientation factors and high crystallinity) were verified by wide-angle X-ray scattering and small-angle X-ray scattering.

The reference works above summarized the improvement of thermal conductivity of polymer with nanometer-size individual fibrils, micrometer size individual fibers, and thin films. The mechanism can be summarized as improving crystal regions, reducing amorphous regions to facilitate phonon propagation inside the polymer. Apart from that, another approach is to mix high thermal conductivity fillers into the composite to improve the thermal conductivity. Lee et. al reported a work mixing epoxy with various high thermal conductivity materials such as boron nitride, silicon carbide whisker, and aluminum nitride, etc. [13]. A work done by Wang [14]

reported that mixing of fluorinated carbon nanotubes and nano fibrillated cellulose composite shows good thermal conductive properties of composite through the facile vacuum-assisted method. The in-plane thermal conductivity is found to be 14.1 W/m-K. A new kind of plastic which is composed of cellulose and functionalized graphene has been studied, and they found a high thermal conductivity in the in-plane direction as high as 9.0 W/m-K [15]. However, these methods are not easy to get controllable thermal conductivity, for instance mixing with an appropriate proportion of high thermal conductivity fillers,applying mechanical drawing, macro heating and stretching on the filament, and so on. In the first part of this work, we produce cellulose filament with high orientation order, and high crystallinity via flow-focusing channel system.

1.4 Fire retardancy materials, a new functional clay-cellulose material for flame retardant.

Flame retardant materials are widely used in where applications that exist the possibility of being threatened by fire such as public buildings, and electrical devices[16]. Halogenated composites that contain bromine and chlorine were used as flame retardant materials via generation of nonflammable gases to terminate the chain in the flame[19,20] and blocking oxidative reactions[17]. However, even halogenated composites were reported with wide use in the market. It also has been reported to form toxins that are bad for humans and the environment [18,19]. Possible candidates to replace halogens are nitrogen and phosphorus compounds[20- 23], where the mechanism is similar to halogen flame retardants; dilative fire retardants systems form a char layer to protect further propagation and insulate the underlayer materials[24]. However, most of these flame retardant materials will reduce mechanical properties.

Clay nanoparticles such as montmorillonite (MTM), which is structured by two silica tetrahedral layers acting as a sandwich octahedral layer, sharing an aluminum or magnesium atom in the center of octahedral structure [29,30], are considered as a suitable material for flame retardant due to its impressive improvement in physical,

mechanical, biodegradability, and flame retardant properties [25]. The mechanism of excellent flame retardant properties of clay-polymer composites was established until 2015: MTM forms a protective surface barrier in taking oxygen and volatiles so that it protects underlying material by thermal insulation.In addition, MTM promotes the formation of carbonaceous char which is not easy to be oxidized [5], [26], [27]. Nano-cellulose is introduced for its high strength (1.6-3 GPa) and high crystalline stiffness (≈ 130 GPa) to improve clay/polymer composites' mechanical properties[5]. In the work reported by Medina et al. [28], nacre-inspired MTM clay/cellulose nanocomposite has shown excellent mechanical properties, with the highest Young's Modules 28 GPa and maximum ultimate strength 280 MPa.

Cellulose nanofiber can be obtained from wood, and it is regarded as one of the most renewable resources. Nano-fibrillated cellulose (NFC) can be obtained via fibrillating from cellulose [29]. NFC is an excellent candidate in the use of thermal management with the highest thermal conductivity up to 2.45 W/m-K [30]–[32], and it is considered as a potential material with high thermal conductivity. This intrinsic high thermal conductivity of NFC brings a new concept for MTM/ polymer flame retardant materials, via reducing the high temperature by modifying the thermal degradation route with the help of high thermal conductivity NCF in one direction to dissipate heat. For all this, pure CNF material is limited by low thermal conductivity, accordingly, studies are needed to improve the thermal conductivity of CNF based material[33]. Cellulose-based polymeric materials are widely used in industries due to good adaptability performances[34]. However, cellulose-based materials are easy to combust due to their intrinsic flammability when it accumulates sufficient heat and encounter oxygen with further leading to combustion[35]. To solve this issue, one method is to remove or reduce heat generation, and the other is to prevent oxygen or volatile access to fire, but these two methods do not solve the issues fundamentally. Modifying the thermal degradation route to lower the temperature gradient is an effective solution [36].

Fu et al. [37] reported nano cellulosic wood scaffold impregnated with colloidal MTM to form a wood hybrid, which was verified with high fire retardancy. Gupta et al. report[38] discussed the fire retardancy of sepiolite clay and cellulose nanofibers based

aerogel. Through introducing clay into cellulose nanofiber to make a composite aerogel, fire retardancy was achieved being tested by horizontal burning test and flame penetration, and thermal conductivity measurements also show good thermal insulation properties of prepared composite aerogel. However, none of these research focuses on the anisotropy ratio of clay/CNF films in the application of high fire-retardant materials. It is essential to establish a framework to understand anisotropic thermal property as thermal degradation will follow a direction through in-plane direction with high thermal conductivity to further lower the temperature of hot spot, and resist heat passing through cross-plane direction with lower thermal conductivity. To explore high thermal conductivity in the in-plane direction, several methods have been implemented, such as mix with aligned fillers (such as MTM) in matrix to form effective thermal paths through in-plane direction, and reduce interfacial thermal resistance between fillers and fillers or fillers and matrix. Among these methods, improving the alignment of fillers is considered as a useful approach to minimize the thermal boundary resistance along in-plane direction.

To fully understand anisotropy thermal properties of MTM/CNF thin films, in this work, we prepared a series of clay/CNF thin films with layer by layer structure via vacuum-assisted assembly method (samples are fabricated by Dr. Lengwan Li, Dr. Lilian Median in Prof. Lars Berglund group at KTH Royal Institute of Technology Wallenberg Wood Science Center at Stockholm, Sweden), and characterize the anisotropic thermal conductivity properties. In contrast with previous studies, we report the highly anisotropic thermal performance in different fractions of clay/CNF compound and clarify the correlation between structure and thermal properties, particularly how the orientation of CNF in 3D directions affect anisotropic ratio under hierarchical clay framework. The results were found that the anisotropy ratio of thermal conductivity reaches as high as 30 times, which is higher than previous research.

1.5 The objective of this thesis.

With the wide use of thermal management materials in industries, green functional

materials with better thermal performance are required. Cellulose-based materials, renewable resources, attract attention due to their excellent mechanical properties and flexibility. To further explore its application, thermal properties need to be investigated. Here in this thesis, first of all, we idenfigy high thermal conductivity cellulose filaments and understand fundamental structural properties that influence the thermal conductivity of filaments. Furthermore, we extend the high thermal conductivity of individual cellulose fibrils to composite materials with flame retardant applications in mind. In overall, we aim to idenfify a broad controllability of thermal conductivity of nano-cellolose material through control of alignments, internal bonding, and composition.

Chapter 2

Well-aligned cellulose filaments with high thermal conductivity via flow focusing channel system

2.1 Flow focusing channel system and preparation technique of cellulose nanofibril

Cellulose nanofibrils can be obtained from forest products, and thus, it is a biodegradable and renewable resource with great potential in various technological applications. To make good use of its thermal and mechanical properties, nanostructures of cellulose fibrils, such as its orientation and interaction, need to be optimizeds. In this work, a flow-focusing channel system developed by our collaborator at KTH [39] is utilized to obtain well-aligned cellulose fibrils via the hydrodynamic effects. Furthermore, the well-aligned cellulose fibrils are gelled with the gelation process with the help of salt or acid in the sheath flow.

In the present experiments, cellulose (0.2 wt % TEMPO CNF) is dispersed in distilled water. The cellulose pulp was purchased from Nippon Paper Group. Before the experiment, it is necessary to obtain well-separated TEMPO cellulose dispersion. the cellulose dispersion is stirred using a magnetic stirrer to blend the dispersion for 10 minutes at 1500 rpm rotational speed. Next, it is homogenized using the equipment homogenizer phytotron at 7500 rpm for 10 minutes. Then, the horn sonicator at 25 mm/mindisperses the CNF for 10 minutes followed by ultra-centrifugation at 7500 rpm for 10 minutes to remove the sedimented impurities to obtain a stable dispersion. The CNF dispersion was stored at a 288 K refrigerator. The basic procedure is summarized in Figure 3.

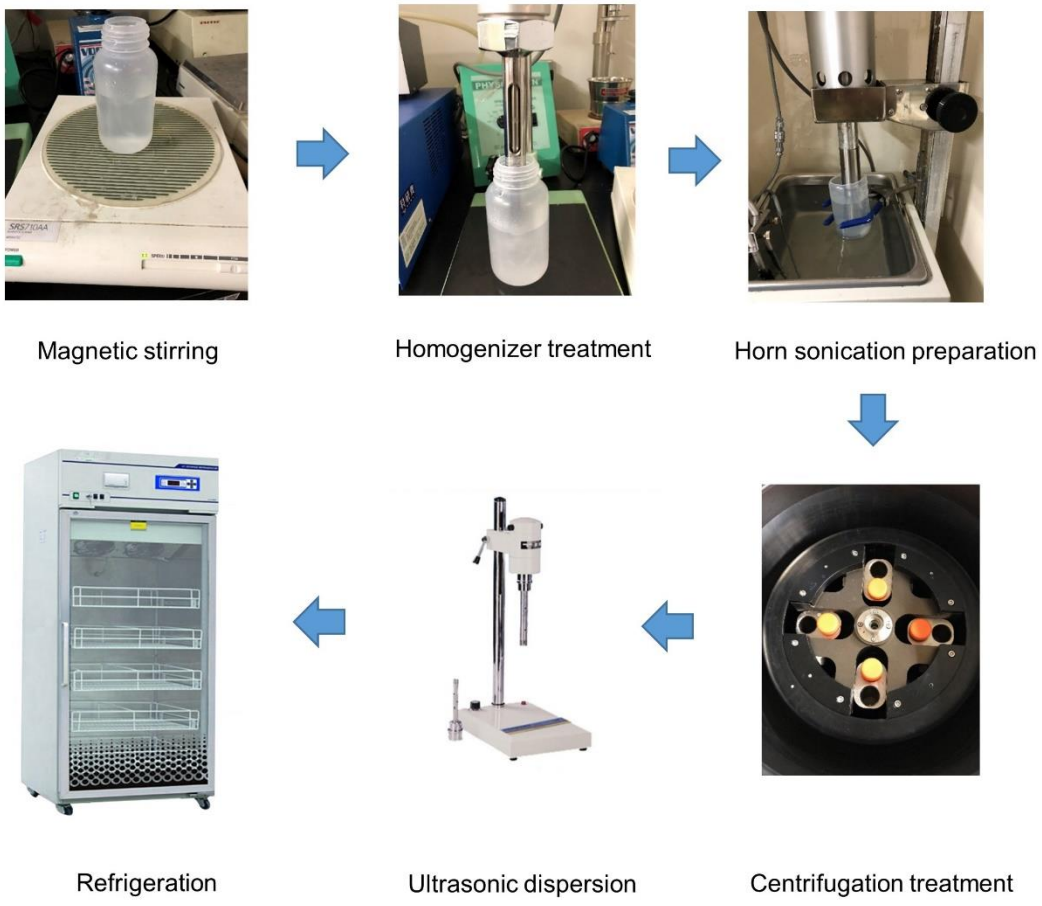

Fig. 3 Cellulose dispersion (0.2 wt %) preparation processes. (a) Magnetic stirring, (b) Homogenizer treatment, (c) Horn sonication, (d) Centrifugation treatment, (e) Ultrasonic dispersion, (f) Refrigeration.

The utilized flow channel is shown in Figure 4, with the cross-section area being 10^{-6} m^2. The channel is made of stainless steel in the middle, fixed with two acrylic plastic sheets of the same size of stainless steel, and locked up with a number of screws. The inlets of cellulose dispersion, distilled water, and salt or acid solution are attached with rubber hoses, to which the syringes are installed to inject the fluids. Before fabricating the ceelulose fillamenets , the channel is purged with distilled water to remove the entrapped bubbles and air inside the channel to avoid impurities vestigial in cellulose filaments.

The TEMPO cellulose dispersion is injected into the core flow, with the flow rate of 4.98 mL/h. At first, the cellulose nanofibrils are free to rotate like rods in the

channel due to the strong electrostatic repulsion effect and are randomly distributed in the channel (i.e. Brownian diffusion [39]). When injecting distilled water at flow rateof 24.88 mL/h into the sheath flow channel 1 (in Fig.4), the flow field changes, and the nano cellulose fibrils become aligned parallel to the axis of the channel (flow direction). With the inclusion of salt or acid via sheath flow channel 2, with a flow rate of 4.15 mL/h, the well-aligned cellulose fibrils become gelled. The gelation is mainly due to the hydroxyl dehydration reaction of cellulose and causing bird nesting between the fibrils. Next, the gelled cellulose filament flows into the ethanol bath. It needs to be noted that all the flow rates are optimized by prior researchers [39] via four timescales: firstly, before sheath flow1, the fibrils are free to rotate (alignment timescale). Next, with the injection distilled water in sheath flow 1, the fibrils becomes aligned with changing the flow field (rotation timescale). In addition, ion concertation to infiltrate into the gelled filament under sheath flow 2 (ion timescale). Finally, gelled filament flow into the bath (convection time scale)..

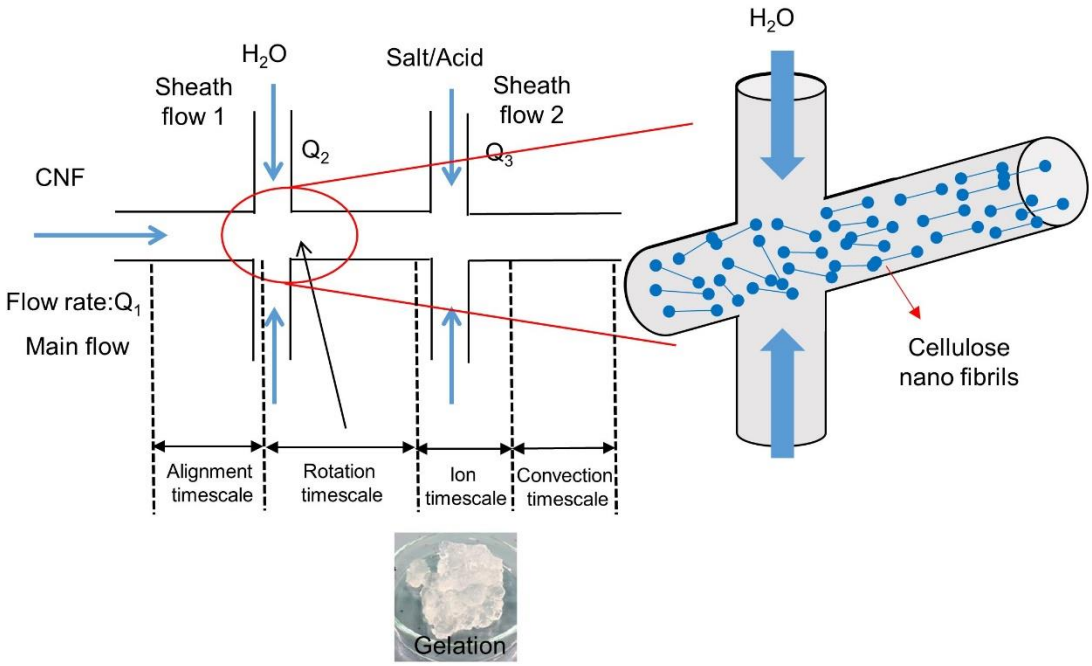

Fig. 4 Schematic diagram of flow-focusing channel system.

The flow rate of different fluids and their concertation are summarized in Table

1. As shown in Fig.4, the core flow injected is cellulose dispersion with 0.2 wt% within alignment timescale range. The sheath flow channel 1 is injected with distilled water, fibrils become aligned within rotation timescale range. In sheath flow channel 2, injected acid or salt are namely hydrochloric acid and ferric chloride with the same concertation of 0.01 mol/L in the range of ion timescale. Hydrochloric acid could help the formation of hydrogen bonding between the cellulose fibrils, and ferric chloride could help the formation of ionic bonding between the fibrils. The gelled cellulose filament flows into a bath filled with ethanol to exchange and quickly evaporate water condensed in the gelled cellulose filaments. After obtaining the gelled cellulose filaments, we put the filaments under room temperature (around 22℃), with relative humidity at around 50% for drying for a period of 24 hours.

Table 1 Summary of details of flow-focusing channel system, including flow rate, the concentration of the solution of core flow, and sheath flow.

<table>
<tr><td></td><td colspan="2">Core flow</td><td>Sheath flow 1</td><td colspan="2">Sheath flow 2</td></tr>
<tr><td rowspan="3"></td><td>Liquid</td><td>Weight %</td><td>Liquid</td><td>Liquid</td><td>Concentration [mol/L]</td></tr>
<tr><td>CNFs</td><td rowspan="2">0.2</td><td rowspan="2">Distilled water</td><td>HCl</td><td rowspan="2">0.01</td></tr>
<tr><td>CNFs</td><td>$FeCl_3$</td></tr>
<tr><td>Flow rate [mL/h]</td><td colspan="2">4.15</td><td>4.98</td><td colspan="2">24.88</td></tr>
</table>

2.2 Thermal conductivity method: T-type method

To estimate the thermal conductivity of cellulose filaments, we perform T-type thermal conductivity measurement. Fujii et al. have measured the thermal conductivity of a single carbon nanotube by using a suspended T-type nanosensor developed to measure millimeter-sized fibers' thermal conductivity[40]. In this technique (in Fig.5), three copper blocks are used as heat sinks and attached to a temperature control plate.

A platinum wire is suspended on two of the copper blocks, attached by silver paste, and then current is applied to the platinum wire, thereby it will generate a temperature increase along the platinum wire due to the well-known Joule heating effect.

By attaching a test sample on the platinum wire (one side of the test sample is connected to the center of platinum wire using thermal glue, and the other side is connected to the third copper block), when applying the current to the platinum wire, the heat will go through the test sample via the middle junction point, and the temperature distribution will be changed. Comparing the cases with and without the test sample, the average temperature increase measured by the average electricity resistance raise, the total heat flux passing through the test filament is estimated. This amount is only the function of platinum length, diameter, the temperature coefficient of resistance, thermal conductivity of hot wire and test filament diameter. Since all the parameters other than the thermal conductivity of the test filament are either known or can be estimated, by fitting the experimental data and theoretical curve, the thermal conductivity of the test filament can be extracted.

Here, the test sample and platinum wire were connected by thermal greasto improve the thermal boundary conductance. To keep the temperature of the whole substrate at the same temperature, we use a temperature controller (OMRON Corporation), and it is connected to a temperature control plate (peltier) to adjust the temperature. The whole device is put in a homebuilt vacuum chamber with all electricity cables connected to the instruments via a flange with interface channels. The vacuum chamber was used to avoid the surrounding air to influence the measurement of thermal conductivity.

2.2.1 Heat transfer model

T-type thermal conductivity is considered as a useful method to obtain the thermal conductivity of fiber materials. Equations (1) and (2) are the one dimensional equation of heat transfer, where $T(x)$ is the temperature distribution along the axis of platinum

wire, T_0 is the temperature of copper blocks, *Q* is the total heat generated by Joule heating, q_0 is the total heat source inside a unit, *k* is the thermal conductivity of platinum wire (which act as hot wire). The *x*-axis is taken in the direction of platinum wire, where the test sample is connected to the middle of the platinum wire at *x*=0, and the positions at the end of two copper blocks are x=$\pm$L/2. A_c is the cross-section area of platinum wire. *L* is the length of platinum wire. *D* is the perimeter of platinum wire. *g* represents the heat loss coefficient.

$$\frac{\partial^2 T(x)}{\partial x^2} + \frac{q_0}{k} = 0 \tag{1}$$

$$q_o = \frac{Q}{A_c L} - \frac{4g}{(T - T_0)D} \tag{2}$$

Here, q_0 represents total heat generated at the entire platinum wire by Joule heating minus the heat loss from platinum wire (including thermal convection in air and thermal radiation to the environment).

When attaching test sample to the middle of the platinum wire on one side and to the copper block on the other side, the heat conductance through test sample, which means the heat passing through test sample should equal to the difference in heat flux between the positions at x=0^+, and x=0^-, as expressed as boundary conditions in Equation (3). Note, since the temperature profile should be continuous, the temperature at both x=0^+ and x=0^- should be the same.

$$\frac{T(0) - T_\infty}{R_{fiber}} = kA_c \left(\frac{\partial T_{x=0+}}{\partial x} - \frac{\partial T_{x=0-}}{\partial x} \right)$$
$$T(x = 0^+) = T(x = 0^-) \tag{3}$$

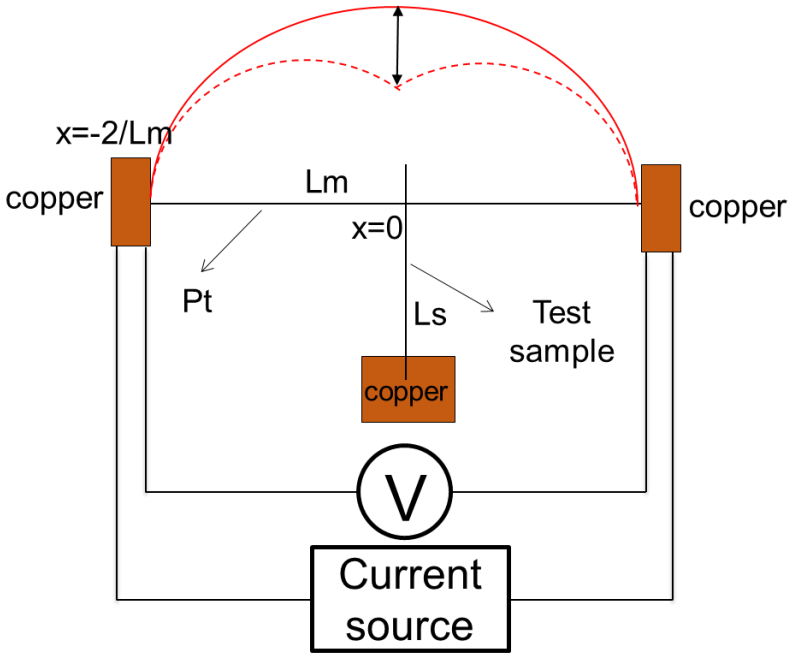

Fig. 5 Schematic diagram of T-type thermal conductivity measurement.

2.2.2 Consideration of heat loss (heat convection and heat radiation)

Since the measurement may be influenced by thermal radiation, an estimation of the heat loss effect is performed before testing the samples. To measure thermal conductivity without the influence of thermal convection, we conducted a vacuum experiment by pumping out the air inside the chamber before the measurement. The working pressure is set to be around 1×10^{-3} Pa based on the estimation that the total conduction of heat is about 75% of total Joule heating under the pressure of 10 Pa and the ratio reaches 88% when the pressure is 1×10^{-1} Pa.

The Equations (1)(2) can be solved for the temperature profile along a single platinum wire. By integrating it along the entire wire, the average temperature increase can be obtained as a function of total Joule heating, heat loss coefficient, and the other parameters of platinum wire. The average temperature increase of hot wire is expressed below.

$$\overline{\Delta T} = \frac{Q}{gLS} - \frac{2Q}{gL^2 S\sqrt{\frac{gS}{kA_c}}} \tanh\left(\sqrt{\frac{gS}{kA_c}}\right) \tag{4}$$

Here, apart from the parameters that have been explained with Equations (1)-(2), S is the total surface area of platinum wire.

As electrical resistance is a function of initial resistance R_0, thermal coefficient of resistance α, and the average temperature increase ΔT.

$$R = R_0[1 + \alpha\overline{\Delta T}] \tag{5}$$

With integrate with equation 4, the theoretical average electrical resistance can be summarized as below:

$$\overline{R} = R_0\left\{1 + \alpha\left[\frac{Q}{gLS} - \frac{2Q}{gL^2 S\sqrt{\frac{gS}{kA_c}}} \tanh\left(\sqrt{\frac{gS}{kA_c}}\right)\right]\right\} \tag{6}$$

In the actual experiment, we applied a current from 0 μA to 200 μA with a small increment of 100 mA, and urther increase the current to 10 mA with larger increment of 200 mA. Then the current is decreased to 0 A in the opposite manner with the same decrement. By plotting square of current vs the ratio of electrical resistance increase, the experimental data and theorrtical data could be compared.

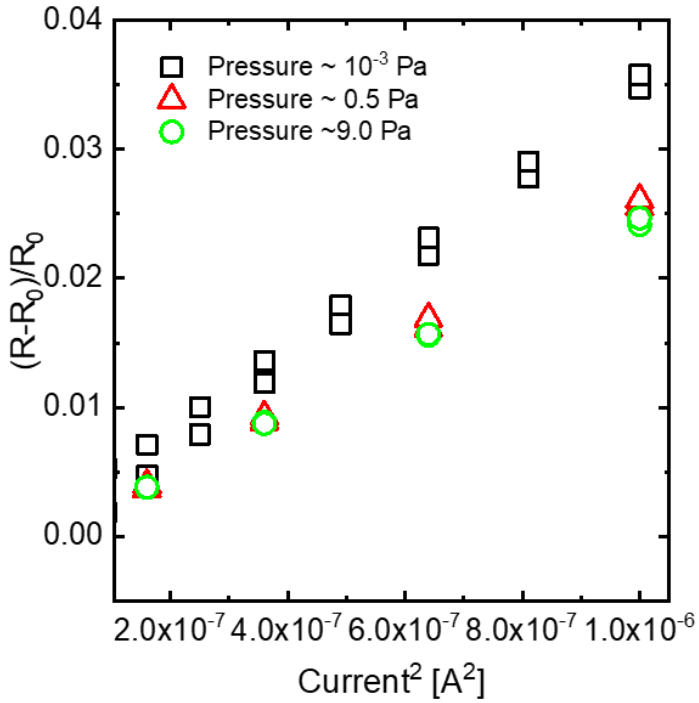

Fig. 6 Electrical resistance rise with increasing current at 1×10^{-3} Pa, 10 Pa, and 9.0 Pa.

In Fig.6, we summarize electrical resistance rise with increasing current under three cases: theoretical data assuming the thermal conductivity of platinum as 85 W/m-K, and experimental data at pressures of 1×10^{-3} Pa and 10 Pa. It is easy to find out that there is a difference between experimental data of 1×10^{-3} Pa and 10 Pa. Based on the approximation that the average temperature rise of platinum wire is 9.6 K in case of 10 Pa, the average experimental temperature reaches 10.9 K, about 1.3 K higher in case of of 1×10^{-3} Pa with the maximum current of 10 mA. The detailed information is summarized in Table 2.

Table 2 Summary of details of heat loss under different pressure conditions.

Pressure [Pa]	TC of Pt measured [W/m-K]	Average temperature increase [K]	Heat loss coefficient [W/m^2K]	$Q_{\_conduction}/Q_{\_total}$
10		9.56	1.243	74.7%
1×10^{-3}	85	10.87	0.555	87.5%

This difference in temperature increase can be attributed to the heat convection, which is less under low pressure. With the size of the chamber and vacuum pump used in the current setup, it usually takes about one hour to research 1×10^{-3} Pa. The experiment setup is shown in Fig. 7. Apart from the equipment that we have explained earlier, it shows the cooling system used for cooling the chamber.

During the measurement, the substrate will also heat up by Joule heating. To avoid the overheating of the substrate, one can either use large size copper blocks as heat sinks or use an active cooling platform under the chamber. We used the cooling system by circulating water at 17 ℃ to maintain the temperature at the base value.

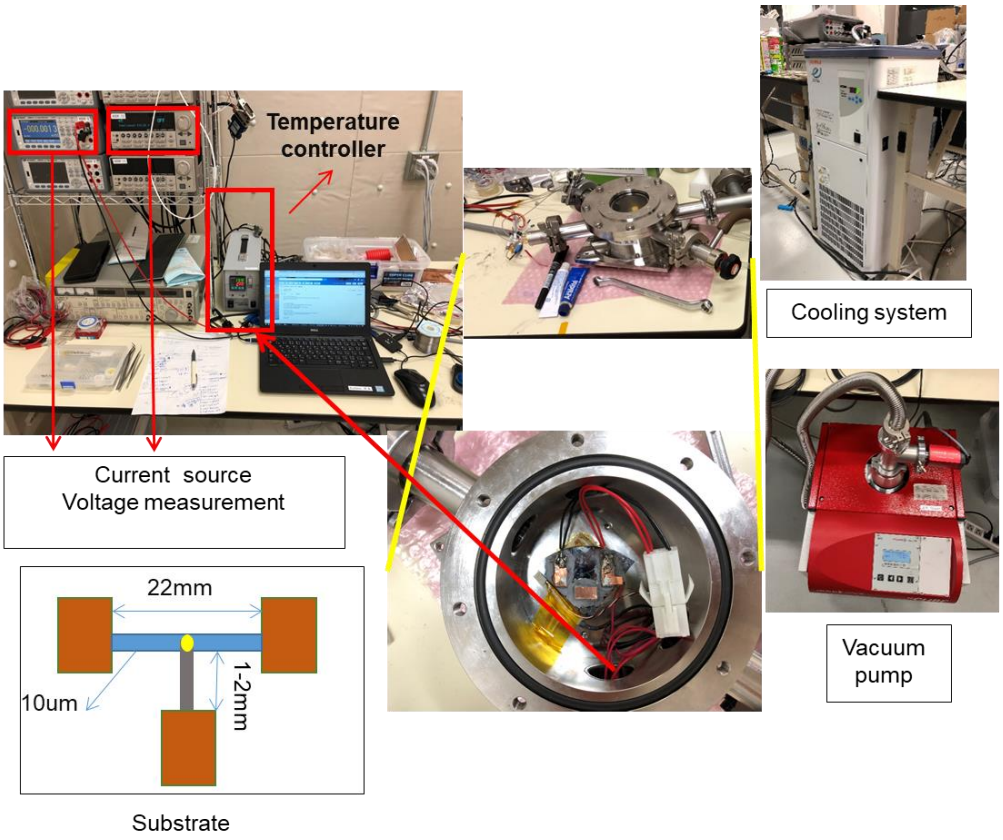

Fig. 7 Pandect experimental setup for measuring thermal conductivity.

To measure the thermal conductivity of the test filament, the thermal conductivity of platinum hot wire should be measured first. The platinum wire length is 25 mm, and the diameter is 10.3 μm. To measure the thermal conductivity, we first increase current from 0 mA to a maximum of 10 mA and then decrease to zero again. At each current value, the current square of average point *vs* resistance curve is obtained as in Fig. 8. By performing this at 293 K, 298 K, and 303 K, three curves can be obtained. The intercept of the curve represents the initial electrical resistance of platinum wire with no supply of current. By extracting the initial electrical resistance R_0 under different temperatures, we can estimate the thermal coefficient resistance α via Equation (7).

$$\alpha = \frac{\Delta R}{R_0 \Delta T} \tag{7}$$

The estimated thermal coefficient resistance α is found at around~ 0.003218/K, which is acceptable compared with the reference value of 0.0034/K [41].

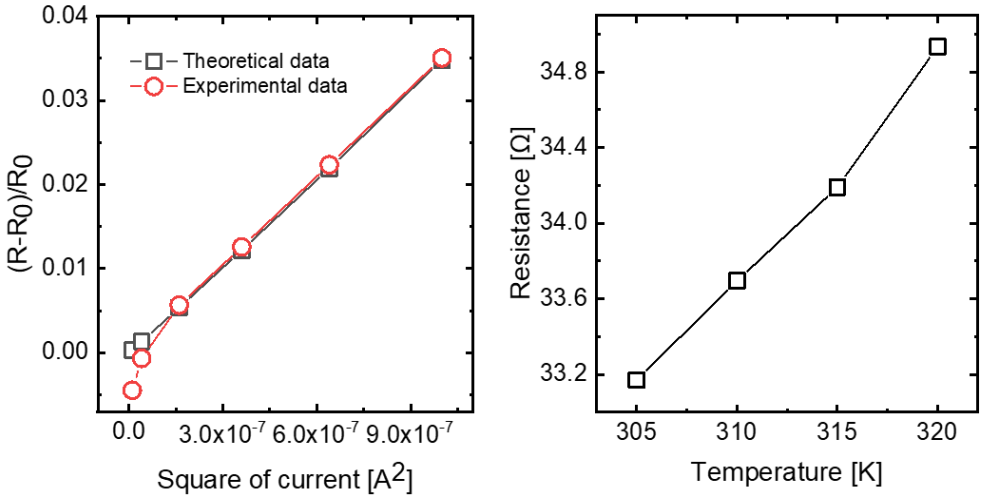

Fig. 8 (a) Current square with electrical resistance increase, (b) Temperature with initial electrical resistance.

By fitting theoretical curve and experimental curve, we obtained the thermal coefficient resistance (TCR) α, and the estimated thermal conductivity of platinum wire is 80 W/m-K at 293 K, which is acceptable compared with the reference value of 78 W/m-K[42].

In order to check the accuracy of T-type measurement, a reference sample should be measured. We take platinum as a reference sample. The test platinum sample with length around 1.5 mm, diameter around 10.3 um was placed at the center of hot platinum wire, connected by thermal glue. By comparing the curve in the case of only Joule heating platinum wire, and hot platinum wire with attaching test platinum, we can extracted the thermal conductivity of the reference platinum sample as well. In the case of maximum current 10 mA, the estimated temperature difference is around 6.2 K under measurement temperature at 293 K. By fitting the curve between theoretical and experimental data, the estimated thermal conductivity of test platinum wire is ~75 W/m-

K.

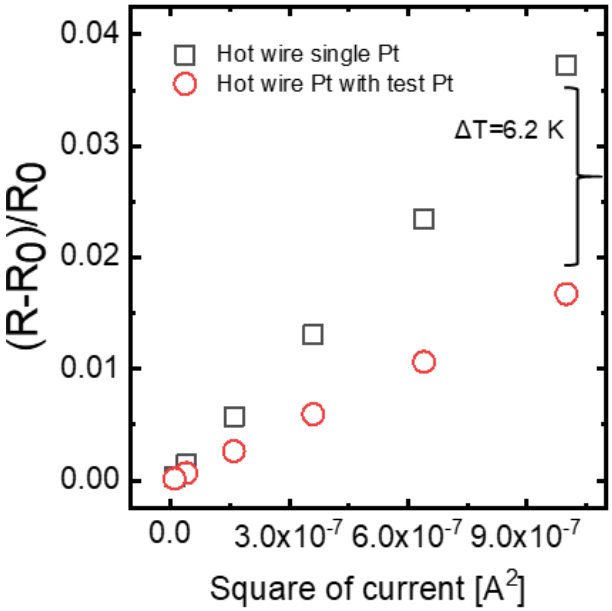

Fig. 9 Electrical resistance increase ratio between the single hot wire and hot wire with test Pt wire measurements at different current values.

We also consider the thermal contact resistance of glue connected between the hot platinum wire and test sample to improve the measurement accuracy. From thermal glue company, the thermal conductivity of thermal glue is around 3 W/m-K. Since only one drop of thermal glue was used, we estimated the thickness of thermal glue is 1×10^{-4} m, and the thermal resistance of thermal glue is around 3×10^{-5} m/W. For a typical cellulose filaments samples with length of 2 mm and thermal conductivity of 5 W/m-K, the estimated thermal resistance is $\sim 4 \times 10^{-4}$ m/W, which is 10 times larger than the thermal glue contact thermal resistance. Therefore, it is safety to ignore the thermal resistance of the thermal glue in the measurement.

Another important factor that need to be considered is the heat loss by radiation through the test filaments. The heat radiation is proportional to the surface area, and it propotional to the fourth power temperature difference between the sample temperature

and the environment temperature. Giving the large surface areas, the radiation loss need to be considered in order to get the correct measured value.

The ratio of heat radiation and total Joule heating can be expressed as below:

$$\frac{Q_{Radiation}}{Q_{total}} = \frac{\varepsilon\sigma A_{surface}(T_{avg}^4 - T_0^4)}{K_{CNF} A_{CNF\_cross} \dfrac{T_{avg} - T_0}{L_{CNF}}} \tag{8}$$

Here, ε represents the emissivity of cellulose filament. The emissivity of cellulose, which is take from reference[43], is 0.85; σ is the Stefan-Boltzmann constant and equals to 5.678×10^{-8} W/m^2-K^4; $A_{surface}$ is the total surface area of cellulose filament; T_{avg} means the average temperature of whole cellulose filament, which is integrated from 0 to the whole length and divided by the total length of sample; T_0 is the temperature at heat tank; A_{CNF_cross} means the average cross-section area of test cellulose filament (we usually make an average value of three measures cross-section area); L_{CNF} means the length of test cellulose filament.

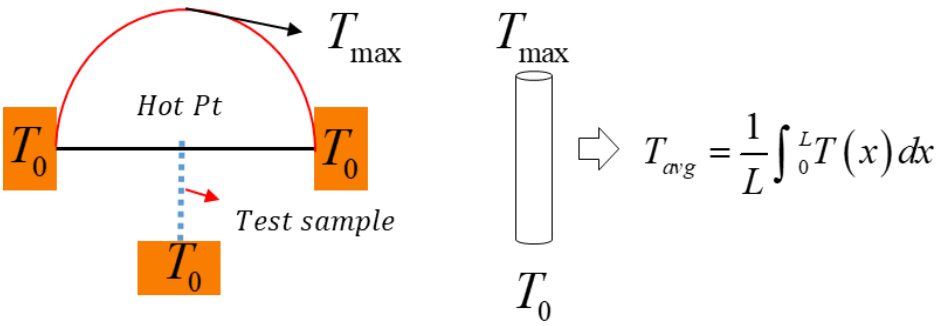

Fig. 10 A simple illustration of the average temperature of the test sample.

Based on the calculation, the heat loss due to radiation through cellulose filament is found to be ~ 21.6% of the total heat conducted through the filament and the estimated thermal conductivity can be set as 14.5 W/m-K, instead of 18.5 W/m-K in case heat radiation through the sample filament is not considered.

Table 3 Summary of details of heat loss due to radiation through CNF filaments.

Emissivity_ CNF	T_{max} [K]	T_0 [K]	$Q_{\_radiation}/Q_{\_total}$	$K_{\_measured}$ [W/m-K]	$K_{\_real}$ [W/m-K]
0.85	304.3	293	21.6%	18.5	14.5

2.3 Mechanical tensile test

In the introduction part, we have reviewed several papers that improve the thermal conductivity of polymer by stretching the polymer film or filaments. Here, we also applied the mechanical tensile on cellulose filaments. The mechanical tensile machine we used is purchased from Shimadzu company, the force sensor we used is a small-scale sensor with a maximum tensile force is 1N. The speed of the sensor in the experiment is set at 5 mm/min, at a low speed with the test piece shape is rod-like pieces. Before the testing, the sample filament is fixed at the clamp carefully, and we use post-it paper to stick the attached test filament, this is due to avoid the slip of the sample from the fixture since our sample filaments are too thin with only 10 um in diameter. After the sample filament is fixed well at the fixture, we calibrates the initial distance and force to be zero. The stretching length of test filaments can be obtained directly from this machine, the diameter information we obtained from the microscope after the stretching.

After all the steps are carried out, we start to break the test filament at the Vibration Reduction Boards. Once the test filament is broken, as detected by the force sensor, the testing is automatically suspended. The tensile strain equals the increasing length divided by the initial length of the test filament. The stress equals the force that is applied on the filaments divided by the cross-section area measured after the breaking.

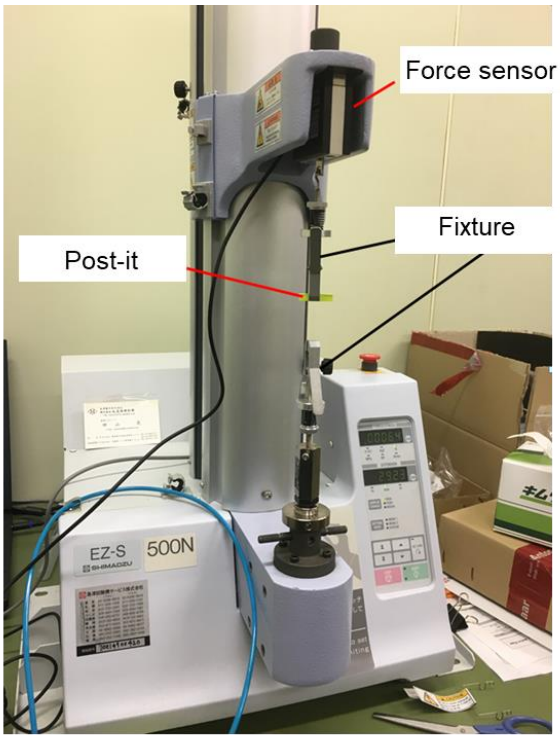

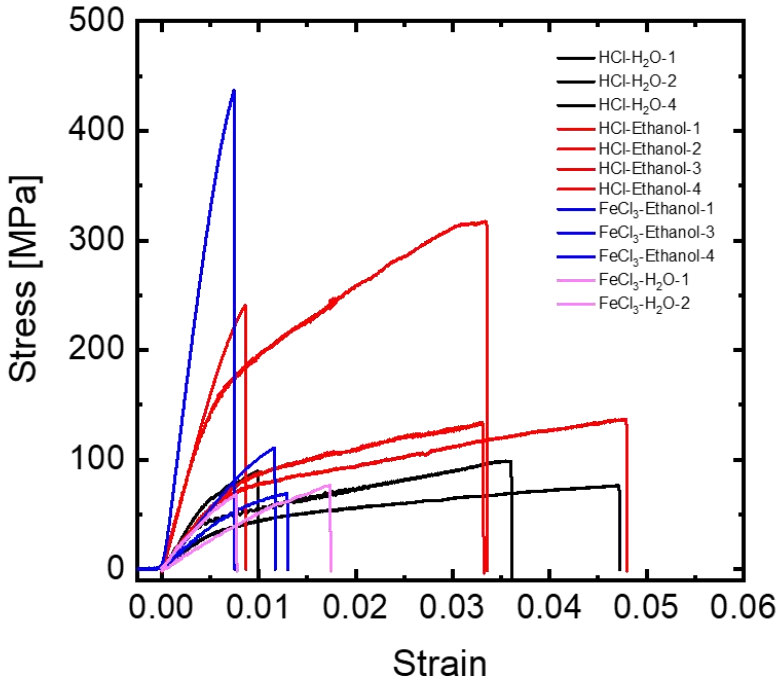

Fig. 11 Strain-stress curve from mechanical tensile test.

The strain and stress curve is shown in Fig.11. We find that with the elongation from zero point, the stress increase with increasing of strain monotonically, until it reached yield strength. After that, the stress increase slowly with further increasing

strain compared with the previous part until it reached the fracture point. [44]

We can also obtain Young's Modulus from the strain-stress curve. Young's Modulus is a parameter that reflects the strain increases with increasing stress with a directly applied force. It equals strain rise divided by stress raise, which is the value of slope in the stain-stress curve. Young's Modulus is an important factor for polymer since it reflects the stiffness which is proportional to the square of sound velocity[45]. As we know that velocity of sound is proportional to thermal conductivity[46], it is critical to investigate the relation between Young's Modulus and the thermal conductivity of the polymer.

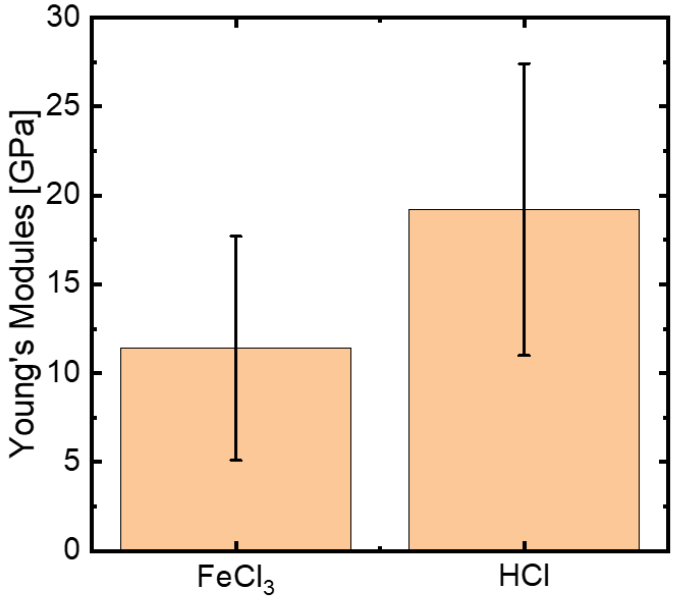

Fig. 12 Young's Modulus of CNF filaments with treated with HCl and $FeCl_3$.

2.4 Cellulose nanofibers crystallinity and orientation characterization

Cellulose fibril structure, interaction, and morphology could influence the thermal properties significantly[47-54]. Numerious characterization methods, such as X-ray diffraction scattering (XRD) [49], nuclear magnetic resonance (NMR) [50], Fourier transform-infrared spectroscopy (FT-IR) [51], and Raman spectroscopy have been used

to characterize cellulose fibrils structure and morphology inside the filaments[48].

In this measurement, we utilize Raman spectroscopy to identify cellulose nano fibrils orientations and crystallinity index. Cellulose is a kind of semi-crystal material, it contains crystal regions and amorphous regions, and crystallinity means the mass percentage of crystalline regions in whole cellulose materials[52]. It is an important factor to influence cellulose materials' properties. Raman spectroscopy has been verified by Isogai group [53] as a useful tool to investigate the crystallinity of cellulose. The residual stress in cellulose fibrils can lead to a shift in the vibration spectra of molecular, atoms, or bonding. These frequency shifts is reflected in the peak shifted of Raman spectra[54].

In Raman measurement, an incident beam coming from the laser is exposed on the surface of test samples, the frequency of the incident beam equals the scattering beam frequency, which is called elastic scattering or Rayleigh scattering, and no elastic collision between the incident photons and test sample molecules occur.

When the incident beam energy is larger than the scattering beam energy, the energy difference of the inelastic scattering happened since the incident photons excite the molecule or atom that is vibrating. This is called Raman scattering. Typically, the incident beam energy minus the energy that causes the exciting molecule from excited position back to the stable position, is used to characterize the movement of the molecular or atom. The energy difference catches and inflects on the Raman shift. The basic mechanism is summarized in the below figure.

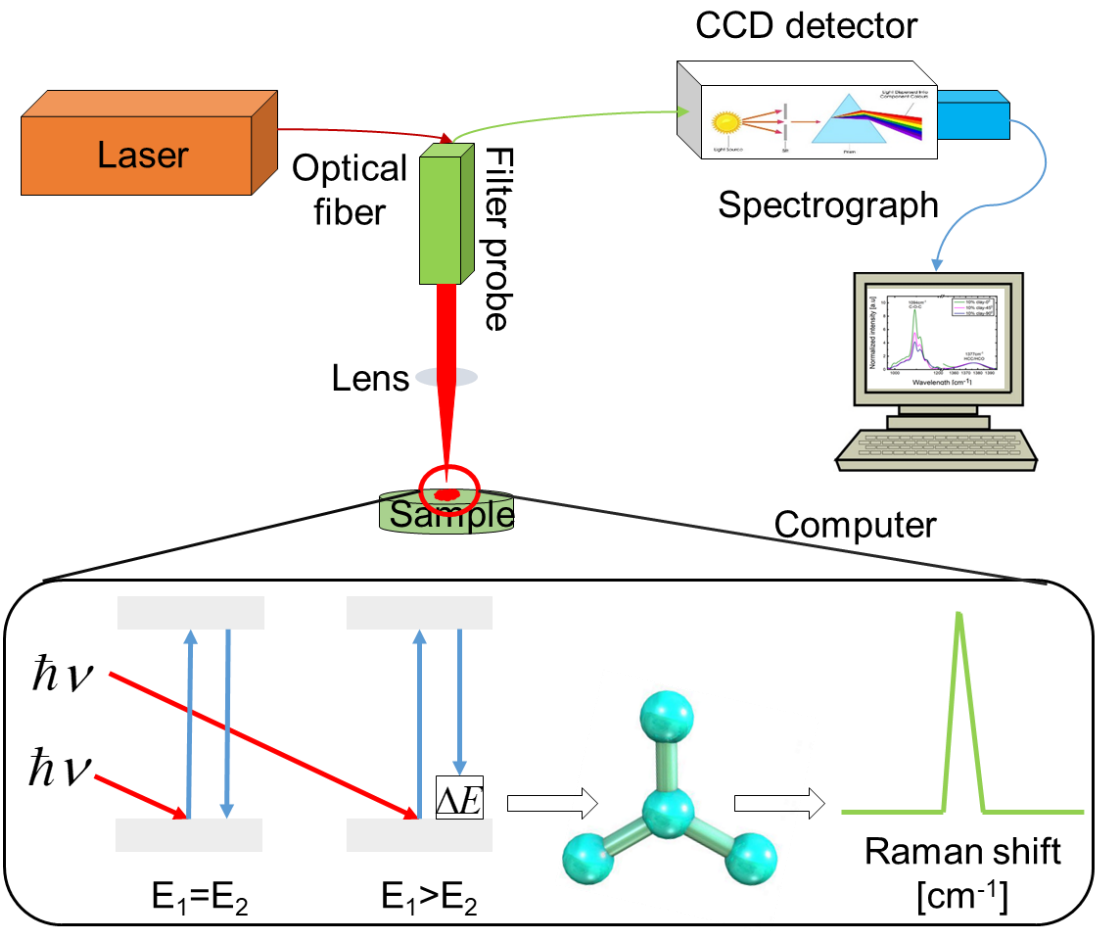

Fig. 13 Diagram of Raman spectroscopy principles.

The Raman equipment used is RENISHAW INVIA. The available continuous waves laser wavelengths are 532, 633, 785, and 1064 nm. The laser wavelength used in this study is 532 nm. A polarized plates is used to selectively turn on/off the polarized of the indicent laser. The grating used is 1800 and 600 with lens VIS and CCD detector. The edge filter is the same as the laser used. Before the measurement, the gratings and edge filters need to be changed to the same as the laser type.

Prior to the production measurement, we used silicon sample to calibraite the setup. The chosen representative peak of silicon is 520.6 cm^{-1} with microscope camera magnification 100 times, 0.1% near-infrared laser state, acquisition exposure time is 30/s for accumulations for 3 times in one measurement. The measured regions are from 30 to 3700 cm-1. The spectrul data was obtained after the substrate the baseline of the initial spectral, and the smoothing process in the software together in the Raman

equipment, and saved into a txt file to do further analysis.

To analyze the crystallinity index, we apply the circular polarized (non-polarized) light in both incident and scattering light. The inelastic scattering of the incident light with the molecular vibraions in the Celluors leads a frequency shift in the Raman spectra, which can be ulitzed to idenfity the underlying vibrational frequency. The vibrational frequency of typical bonds such as C-C-O, C-C-C, C-O, C-C-H, C-O-C have been well studied by Raman measurement [55]. For instance, the peak of cellulose at around 1600 cm^{-1} usually represents the vibration of lignin, since lignin contains a lot of benzene ring, and lignin is a product from the preparation of cellulose so that it is also appeared in cellulose measurement signals[55]. The peak at 380 cm^{-1} represents the C-C-C, C-C-O, C-O ring deformation (glucose ring feformation), which is for the ring in the cellulose molecular[56]. The peak at 1095 cm^{-1} represents the C-C or C-O atoms stretching, which is along the cellulose chain of molecular[57]. The peaks at 2868, 2885, 2941, and 2965 cm^{-1} represent C-H and CH_2 stretching which are on the rings of the cellulose molecules. The peaks at 3291, 3334, 3361, and 3395 cm^{-1} represent the band assignment of O-H stretching, which are outside of the rings of cellulose[57].

During Raman measurement, one cellulose filament was placed under the microscope with 100X amplification focus lense to focus the laser on the surface of cellulose filament. We then extract the crystallinity information of cellulose from Raman microprobe assignments. We suppose that the Raman spectra will not be changed with changing the incident or scattering light of polarization when the cellulose nano fibrils orientations are varied.

Polarization is important in optical measurement since it is the response of a beam of light in certain direction. Therefore optical measurement devices such as devices control the direction of polarizations. If the direction of a beam light is parallel to X-axis, and the oscillation direction of this beam light is parallel to Y-axis, and the movement of light keeps parallel to the X-axis, and it is called is polarized light.

In general, there are three types of polarized light, namely linear polarization, circular polarization, and elliptical polarization. Linear polarization describes the

propagation of light in a perpendicular direction of oscillation. Circular polarization refers to two perpendicular plane waves with the same amplitude, i.e., the planes of the two waves are perpendicular to each other. In addition, circular polarization can be divided into left circular polarization and right circular polarization, depending on the orientation of the two wave plates. Elliptical polarization is similar to circular polarization in that it is two perpendicular waves, but with different amplitudes in the perpendicular plane, and the shape observed from the line of sight in the direction of light propagation is an elliptical shape. This is a typical condition of circular polarization. A detailed description can be understood by the following figures.

In many studies, the polarization of light is required for different purposes. There are many devices to polarize the direction of light, such as waveplates. The purpose of using wave plates is to change the polarization conditions of light. Usually, half and quarter-wave plates are used. Half wave plates are used to change the direction of linearly polarized light into the direction of reverse linearly polarized light. A quarter-wave plate is used to get circularly polarized light from the source linearly polarized light, or linearly polarized light from the source circularly polarized light , in case of Fig.14, convert linear polarized light into circular polarized light by using half wave plate. The wave plate plays an important role in optical measurements because it provides the possibility to polarize the initial state of light. Other useful technical devices, such as fiber optic polarizers, are also important because they filter the light passing in a specific direction and leave the light in other directions outside the polarizer.

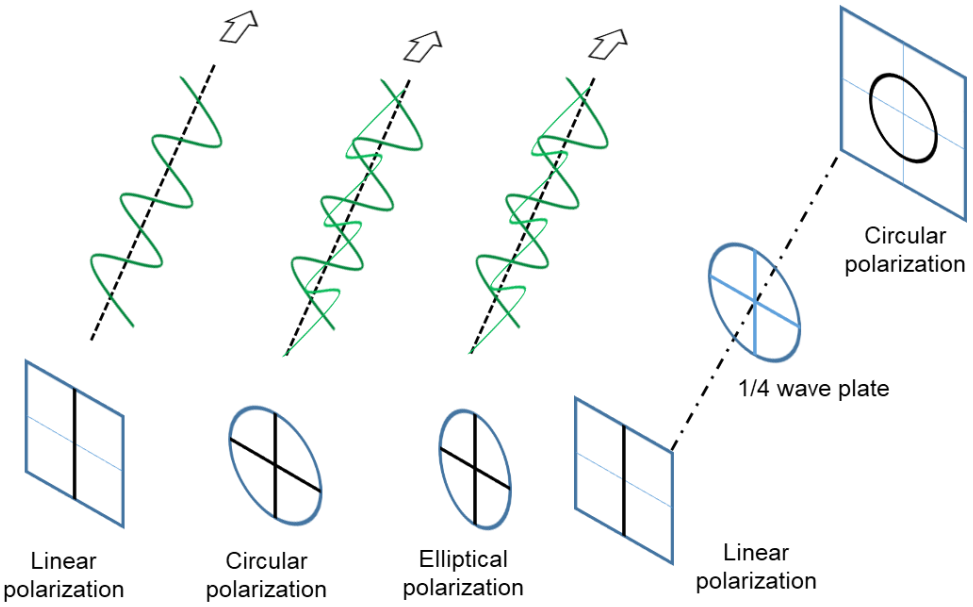

Fig. 14 Diagram of linear polarization, circular polarization, elliptical polarization, and 1/4 wave plate to convert linear polarization into circular polarization.

In the actual Raman measurement, the incident laser beam is linear polarized, we use 1/4 wave plate to convert it into a circularly polarized beam at scattering light (in the filter) in the characterization of crystallinity as illustrated in Fig.14.

Fig. 15 is a Raman spectrum (633 nm laser) of linear polarized light with circular polarization scattering light, acquisition exposure time is 30 s for accumulations for 3 times in one measurement range from 80-3500 cm^{-1} for cellulose filament treated with HCl. From this figure, we can easily observe the typical peaks for instance peak at 1095 cm^{-1} represent the C-C or C-O atoms stretching, peak at 380 cm^{-1} represent the C-C-C, C-C-O, and C-O ring deformation (glucose ring feformation).

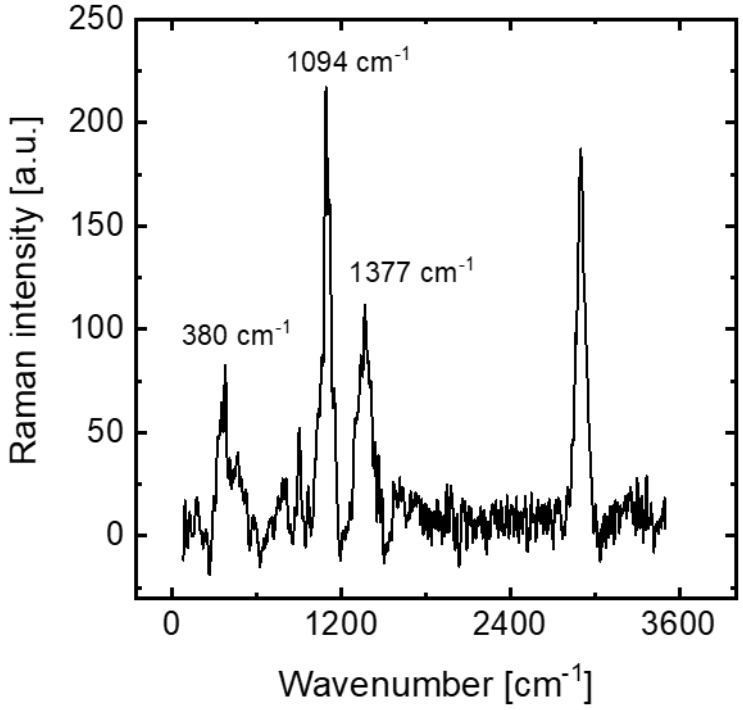

Fig. 15 Diagram of cellulose filament Raman spectral with circular polarization.

To estimate the crystallinity of cellulose materials, the changes in the frequency range of 250-1650 cm^{-1} in the Raman spectral are investigated, especially for the two representative peaks at frequency of 380 cm^{-1} and 1096 cm^{-1}. The shape and height of those two peaks changes significantly at different crystallinity levels[52]. Previous work also found that the shape of 380 cm^{-1} and 1096 cm^{-1} were changed with different crystallinity of cellulose by using ball milling methods[52].

As mentioned in the previous part, the 380 cm^{-1} peak represents the ring deformation of C-C-C, C-O, or C-C-O of cellulose, and the 1096 cm^{-1} peak represents the vibration of C-O-C which connects two glucose cyclic molecules, and it is the same as the indication of cellulose main chain direction. The intensity ratio of 380 cm^{-1} and 1096 cm^{-1} is used to indicate the crystallinity index of cellulose. Here we define the crystallinity index of cellulose as:

$$Crystallinity\ index = \frac{I_{380}}{I_{1096}} \tag{9}$$

Figure 16 shows several typical peaks of 380 cm^{-1} and 1096 cm^{-1} in Raman spectra.

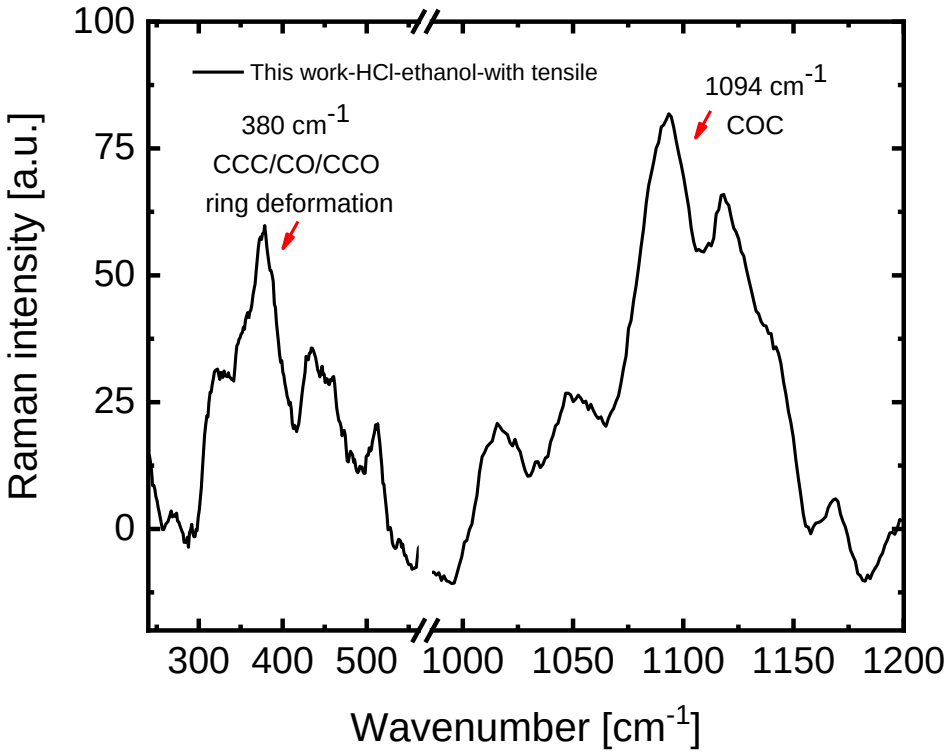

Fig. 16 Diagram of cellulose filament Raman spectra at two typical positions 380 cm^{-1} and 1096 cm^{-1}.

A similar approach to estimate the crystallinity of cellulose has also been used in the previous work[52]. First, they choose different kinds of cellulose samples with different crystallinity and estimate the crystallinity which equals the region of crystal divided by region of amorphous. It was shown that the ratio of 380 cm^{-1} and 1096 cm^{-1} serves as good measure of the crystallinity of cellulose compared with data the standard data obtained from Wide-Angle X-ray Diffraction (WXRD)[58].

Moreover, Umesh et al. [59] measured crystallinity of 41 kinds of biomaterials including sapwoods, heartwood versus sapwoods, and agricultural fibers. The measurement was done by Near-IR FT-Raman and Wide-angle X-ray diffraction. Peaks at 380 cm^{-1} and 1096 cm^{-1} are extracted after horizontal the baseline of Raman spectral.